J. Fluid Mech. (2025), *vol.* 1010, A13, doi:10.1017/jfm.2025.313

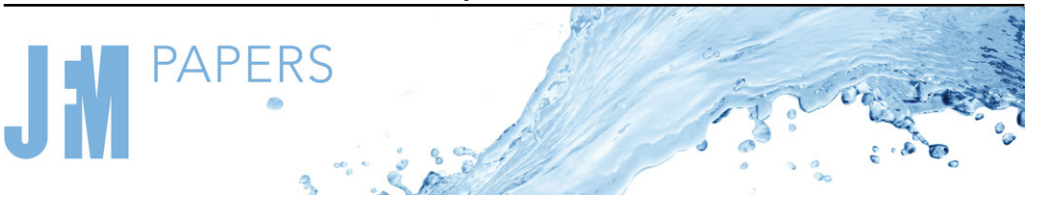

A log-layer analogy for fluid acceleration in the inner layer of wall-bounded turbulence with pressure gradients

Peng E.S. Chen[1], **Wen Zhang**[1], **Minping Wan**[1], **Xiang I.A. Yang**[2], **Yipeng Shi**[3] **and Shiyi Chen**[1,4]

[1]Department of Mechanics and Aerospace Engineering, Southern University of Science and Technology, Shenzhen 518055, PR China

[2]Mechanical Engineering, Pennsylvania State University, State College, PA 16802, USA

[3]State Key Laboratory of Turbulence and Complex Systems, Beijing 100871, PR China

[4]Eastern Institute for Advanced Study, Eastern Institute of Technology, Ningbo 315200, PR China

Corresponding authors: Minping Wan, wanmp@sustech.edu.cn; Wen Zhang, zhangw6@sustech.edu.cn; Xiang I.A. Yang, xzy48@psu.edu

(Received 18 March 2024; revised 30 January 2025; accepted 17 March 2025)

History effects play a significant role in determining the velocity in boundary layers with pressure gradients, complicating the identification of a velocity scaling. This work pivots away from traditional velocity analysis to focus on fluid acceleration in boundary layers with strong adverse pressure gradients. We draw parallels between the transport equation of the velocity in an equilibrium spatially evolving boundary layer and the transport equation of the fluid acceleration in temporally evolving boundary layers with pressure gradients, establishing an analogy between the two. To validate our analogy, we show that the laminar Stokes solution, which describes the flow immediately after the application of a pressure gradient force, is consistent with the present analogy. Furthermore, fluid acceleration exhibits a linear scaling in the wall layer and transitions to logarithmic scaling away from the wall after the initial period, mirroring the velocity in an equilibrium boundary layer, lending further support to the analogy. Finally, by integrating fluid acceleration, a velocity scaling is derived, which compares favourably with data as well.

Key words: turbulent boundary layers

1. Introduction

The study of turbulent boundary layers (TBLs) is a fundamental aspect of turbulence research: TBLs enhance momentum and heat transfer rates compared to their laminar

counterparts, and play a significant role in determining the aerodynamic performance of aircraft, turbomachines, wind turbines, and underwater vehicles. There has been much work on zero-pressure-gradient (ZPG) TBLs (George & Castillo 1997; Smits *et al.* 2011), reaching a consensus on the scaling of the velocity in the overlap region (Marusic *et al.* 2013):

$$U^+ = \frac{1}{\kappa}\ln(y^+) + B \quad \text{for } 1 \ll y^+, \ y/\delta \ll 1, \tag{1.1}$$

where U is the mean velocity, y is the wall-normal coordinate, $\kappa \approx 0.4$ is the von Kármán constant, $B \approx 5$ is another constant, δ represents an outer length scale, such as channel half-height, boundary layer height or pipe radius, and the superscript $+$ denotes normalisation by the viscous units u_τ and $\delta_\nu = \nu/u_\tau$. Furthermore, $u_\tau = \sqrt{\tau_w/\rho}$ is the friction velocity, ν is the kinematic viscosity, τ_w is the wall-shear stress, and $\rho \equiv 1$ (unit) is the fluid density. The scaling in (1.1), known as the logarithmic law of the wall, involves only local flow variables, and will be termed 'velocity scaling in its conventional sense' in this paper.

The existence of the law of the wall relies on the existence of an inner layer (Pope 2000), within which we have

$$0 = \frac{\partial}{\partial y}\left(\nu\frac{\partial U}{\partial y}\right) - \frac{\partial \langle u'v' \rangle}{\partial y}, \tag{1.2}$$

where the left-hand side represents the material derivative $\mathrm{d}U/\mathrm{d}t$ and is 0, and the right-hand side contains the viscous stress and the Reynolds stress terms. Here, u' and v' are the velocity fluctuation in the streamwise and wall-normal directions, and $\langle\cdot\rangle$ denotes an ensemble average. By regarding the Reynolds stress as a 'stress' (rather than fluid motion), (1.2) suggests that the net force in the inner region is approximately 0.

The complexity of TBLs increases significantly under the influence of pressure gradients (PGs). PG TBLs are encountered on aircraft wings during takeoff and landing, around the curved surfaces of wind turbine blades, and on the rear sections of underwater vehicles. The presence of a PG can induce flow separation, impacting stability, lift and drag characteristics (Simpson 1989). Such PG TBLs have also been the focus of many works. However, unlike their ZPG counterparts, there is no well-established velocity scaling for PG TBLs.

Before any discussion on the velocity scaling for PG TBLs, a more fundamental question is the existence of a region where a velocity scaling in the conventional sense can exist. As the net force on a fluid parcel is no longer 0 in PG TBLs, Newton's second law dictates

$$F = ma \tag{1.3}$$

and

$$\Delta U = \int a\,\mathrm{d}t = \int F/m\,\mathrm{d}t. \tag{1.4}$$

Thus fluid velocity or the change therein becomes a cumulative function of the net force over time, rather than being directly correlated to the local force. Here, F is the net force on a fluid parcel, including the imposed PG and the viscous and Reynolds stresses, m is the mass of the fluid parcel, a is the acceleration of the fluid parcel, and t is time.

Perry *et al.* (1966), among others, posited the existence of a region in PG TBLs where the velocity is determined locally. They divided the PG TBL into a 'wall region' and a 'history region'. In the wall region, a velocity scaling in its conventional sense exists. Although the exact mechanism of a wall region is still a research topic, its existence can

be argued through the concept of (quasi)-equilibrium boundary layers (EBLs). Kader & Yaglom (1978) argued that a TBL is in equilibrium if the freestream velocity U_∞ and the PG P_x vary slowly in the flow direction. Townsend and Mellor & Gibson introduced self-similarity of the mean velocity defect as the criterion for equilibrium (Mellor & Gibson 1966; Townsend 1976), showing that the flow is at equilibrium if the freestream velocity follows the power law $U_\infty = C(x - x_0)^m$, where C is a constant, x_0 is a virtual origin, and the power law exponent is $m > -1/3$. It follows from this definition that some types of favourable PG (FPG) TBLs and mild adverse PG (APG) TBLs are at equilibrium (Skote *et al.* 1998; Lee & Sung 2009; Lee 2017). Evidently, ZPG TBLs are at equilibrium as well (Schlatter *et al.* 2009; Bailey *et al.* 2013). In these flows, a wall region exists, and the velocity can be expressed using local flow variables.

This study addresses primarily large APGs, and a wall region is not essential. Nonetheless, examining existing literature on the topic will be instructive. Perry *et al.* (1966), alongside other researchers (Galbraith *et al.* 1977; Alving & Fernholz 1995; Johnstone *et al.* 2010), have documented the persistence of the logarithmic law of the wall in the wall region, albeit with a diminished logarithmic region compared to ZPG TBLs (Monty *et al.* 2011; Vinuesa *et al.* 2014). Monkewitz & Nagib (2023) and Vishwanathan *et al.* (2023) observed variations in the constants of the logarithmic law as influenced by the PG. Moreover, Monkewitz & Nagib (2023), among others (Yang *et al.* 2015; Luchini 2017; Lv *et al.* 2021), have explored the inclusion of a linear term in the velocity scaling. In addition to the logarithmic law and its variations, some studies have identified a half-power law prevailing above the logarithmic region (Stratford 1959; Perry *et al.* 1966; Kader & Yaglom 1978; El Telbany & Reynolds 1980; Coleman *et al.* 2018). Wei *et al.* (2023) further established a scaling law for velocity in the wall-normal direction. Efforts to unify velocity scalings across the viscous sublayer, buffer layer, logarithmic layer and square-root layer have also been reported, contributing to a more cohesive understanding of velocity dynamics in TBLs (Materny *et al.* 2008; Dróżdż *et al.* 2015; Knopp *et al.* 2021; Knopp 2022; Romero *et al.* 2022*a*,*b*; Subrahmanyam *et al.* 2022).

While (quasi-)equilibrium is not hard to fathom at the limit of ZPG, Bobke *et al.* (2017), among others (Vinuesa *et al.* 2017; Parthasarathy & Saxton-Fox 2023), highlighted clear history effects in PG TBLs, even at moderate PGs, challenging the existence of a wall region, and by extension, the existence of any velocity scaling in the conventional sense. For instance, Bobke *et al.* (2017) found that the velocity profiles in two TBLs differ due to different histories of the imposed PG even though the Clauser PG parameters and the friction Reynolds numbers match. In light of this significant role of history effects and the complexity of flow history itself, Pozuelo *et al.* (2022) proposed to establish a family of baselines for non-equilibrium PG TBLs . They followed Clauser (1954) and suggested that a good baseline could be PG TBLs where the Clauser PG parameter

$$\beta = \frac{\delta^* P_x}{\tau_w} \tag{1.5}$$

does not change, where δ^* is the displacement height, and P_x is the PG. It is worth noting that velocity profiles in such PG TBLs were termed 'equilibrium profiles' by Clauser (1954), which is a rather odd use of the word 'equilibrium'. In the same paper, Clauser also defined EBLs as TBLs for which the profiles are identical when $(U - U_\infty)/u_\tau$ is plotted against y/δ, which is a more typical use of the word 'equilibrium'. This paper does not involve or need the concept of equilibrium, but it is still instructive to know that the word has different bearings in different papers and even in the same paper. Reynolds number effect is also critical. The increasing Reynolds number was known to lead to a

decreasing APG effect (Sanmiguel Vila *et al.* 2017; Tanarro *et al.* 2020; Pozuelo *et al.* 2022; Deshpande *et al.* 2023).

Given the difficulty in defining any velocity scaling in the history region, there is limited discussion on the behaviours of the velocity scaling therein. Chen *et al.* (2023*a*) seems to be the only work that claimed to have found a velocity scaling in the history region. In that work, the authors proposed a velocity transformation that maps the velocity profiles in the history region back to the logarithmic law of the wall. The transformation contains an integral of the total shear stress, through which it accounts for history effects in the flow. However, since the integral cannot be evaluated locally, the potential utility of the velocity transformation in turbulence modelling is limited.

Based on this literature review, we may conclude the following. The existing literature predominantly focuses on velocity: on the one hand, velocity scaling in the conventional sense can be anticipated in the wall region, although the exact form of the scaling is still a research topic; on the other hand, no velocity scaling in the conventional sense exists in the history region. This study moves away from the conventional velocity analysis to focus on fluid acceleration, i.e. $\bar{D}U/\bar{D}t$ and its scaling in PG TBLs. In particular, our approach involves making an analogy between the velocity in a ZPG boundary layer and the fluid acceleration in a PG boundary layer.

In preparation for the ensuing discussion, we highlight several key considerations. First, from the standpoint of turbulence modelling, APGs present a more compelling subject of study than FPGs. Perry *et al.* (1966) noted that the existing wall law is adequate for FPG TBLs. Kays *et al.* (1980) demonstrated that models based on a ZPG boundary layer wall law work well under conditions of strong acceleration and very mild deceleration, with discrepancies primarily emerging in scenarios involving APGs – a finding recently reaffirmed by Volino (2020). Spalart & Watmuff (1993) further articulated the greater practical and theoretical relevance of APGs over FPGs. In alignment with this research trajectory, our study will concentrate on large APGs, where the presence of a wall region is not anticipated. Second, we introduce the laminar Stokes solution (Schlichting & Gersten 2016), which is a very good approximation of the mean flow when a fully developed channel flow is subjected to a suddenly imposed PG, although for a limited time:

$$\frac{U}{At} = 1 + \frac{2}{\sqrt{\pi}}\,\hat{y}\exp(-\hat{y}^2) - (1+2\hat{y}^2)\,\mathrm{erfc}(\hat{y}). \tag{1.6}$$

Here, A is the bulk fluid acceleration, $\hat{y} = y/(2\sqrt{\nu t})$ is a self-similarity variable, and $\mathrm{erfc}(\cdot)$ denotes the complementary error function. Finally, we note that the method of analogy is prevalent in turbulence research, drawing parallels between turbulent phenomena and other more well-understood physical phenomena, both within and beyond the field of turbulence. Examples include: the Reynolds analogy, which relates the turbulent transfer of momentum to the turbulent transfer of heat (So & Speziale 1999); Prandtl's mixing length theory, which attempts to model the turbulent viscosity using an analogy to molecular viscosity (Prandtl 1925; Bradshaw 1974); the Raupach's mixing layer analogy, which relates the mixing layer and the shear layer formed at the top of surface roughness in rough-wall boundary layers (Raupach *et al.* 1996; Zhang *et al.* 2022); and the analogy between the turbulent transient channel flow experiencing a step increase in its Reynolds number and the laminar–turbulent bypass transition (He & Seddighi 2013, 2015). The analogy in He & Seddighi (2013, 2015) highlights parallels between temporally evolving channel flow and spatially developing boundary layer flow, and as we will see, is particularly relevant to this study. A similar process was found in rapidly accelerating/decelerating turbulent pipe flows (He *et al.* 2016; Guerrero *et al.* 2023).

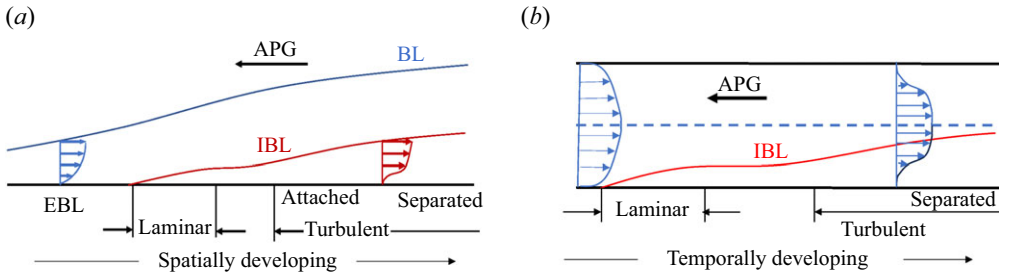

Figure 1. Schematic of the model problem: (*a*) the spatially developing boundary layer (BL) flow subjected to an APG; (*b*) the temporally evolving channel flow with an APG. The IBL is initially laminar, then transitions to turbulence, and may eventually separate.

Taylor & Seddighi (2024) extended the analogy in He & Seddighi (2015) to the turbulent channel with intermediate- and low-frequency pulsations.

The rest of the paper is organised as follows. The model problem is described in § 2. Details of the log-layer analogy are presented in § 3, with validation results in § 4. Finally, concluding remarks are given in § 5.

2. Model problem

Consider the scenario of a spatially developing TBL influenced by PGs. The complexity arises from the turbulent nature of the flow and from the potentially complex patterns of the PG force, which may be represented as

$$P_x = P_0 + \sum_i P_i \cos(k_i x + \phi_i), \tag{2.1}$$

where P_x is the PG force, P_i is the amplitude, k_i is the wavenumber, x is the streamwise coordinate, and ϕ_i is a phase. Analysing the interplay among the many scales that make up the PG and the many scales in a boundary layer presents a considerable challenge – and is unnecessary. Here, we limit ourselves to a constant PG

$$P_x = P_0. \tag{2.2}$$

The model flow problem is illustrated in figure 1(*a*), depicting an initial EBL subjected to an APG. This leads to the development of an internal boundary layer (IBL) (Smits & Wood 1985; Baskaran *et al.* 1987; Garratt 1990; Li *et al.* 2022). The IBL is initially laminar, and its behaviour can be described by the Stokes solution. It then undergoes a transition before becoming turbulent downstream, where flow separation may occur.

The discussion thus far has centred on spatially developing boundary layers; however, the principles discussed are equally applicable to temporally evolving boundary layers. Temporal simulations, particularly of wakes and mixing layers – which are traditionally conceptualised as spatially developing phenomena – have demonstrated considerable effectiveness (Brucker & Sarkar 2010; de Stadler *et al.* 2010; de Bruyn Kops & Riley 2019; Li *et al.* 2024). Particularly relevant to this study is the exploration of temporal simulations as alternatives to spatially developing ZPG TBLs in Kozul *et al.* (2016). Additionally, temporal simulations of PG TBLs have been reported, notably in studies by He & Seddighi (2015), Mathur *et al.* (2018) and Lozano-Durán *et al.* (2020), where a common focus is on the dynamics of a fully developed channel flow when subjected to a suddenly imposed PG. In the context of temporal PG TBLs, as illustrated in figure 1(*b*), the representation of the

PG force adapts to incorporate time, leading to

$$P_x = P_0 + \sum_i P_i \cos(f_i t + \phi_i'), \quad P_x = P_0 \tag{2.3}$$

instead of (2.1) and (2.2). Here, f_i is the frequency.

Comparing a PG TBL and an accelerating or decelerating channel, the most notable difference lies in the outer length scale. In a PG TBL, the outer length scale evolves with the flow, whereas in a channel, it remains fixed at the channel half-height. This difference becomes more pronounced when the flow encounters an APG. The PG induces a negative $\partial U/\partial x$, and due to continuity, a positive $\partial V/\partial y$. The resulting increase in wall-normal velocity thickens the boundary layer, producing a 'straining effect' in the outer layer (Coleman *et al.* 2000, 2003). However, the thickening of the boundary layer has minimal influence on the properties of the inner layer, as the inner layer, by definition, is independent of the outer scale. Consequently, an analogy can be drawn between the inner layer of the spatially developing boundary layer and that of the temporally developing boundary layer. The focus on the inner layer here is motivated by the emerging paradigm of computational fluid dynamics for fluids engineering, where turbulence in the outer layer is resolved directly, and the flow in the wall layer is modelled – often via some sort of mean flow scaling (Bose & Park 2018).

3. Theory

In this section, we present the analogy between the velocity in a ZPG TBL and the flow acceleration in a PG TBL.

3.1. *The log-layer analogy*

We begin by examining the mean flow equation

$$\frac{\bar{D}U}{\bar{D}t} = -P_x + \nu\frac{\partial^2 U}{\partial y^2} - \frac{\partial \langle u'v' \rangle}{\partial y}. \tag{3.1}$$

Here, $\bar{D}/\bar{D}t = \partial/\partial t + U\,\partial/\partial x + V\,\partial/\partial y$ is the mean substantial derivative (Pope 2000). In the absence of any PG force, the equation above becomes

$$\frac{\bar{D}U}{\bar{D}t} = \nu\frac{\partial^2 U}{\partial y^2} - \frac{\partial \langle u'v' \rangle}{\partial y}, \tag{3.2}$$

and it describes the development of a ZPG boundary layer. Define fluid acceleration

$$g = \frac{1}{A}\frac{\bar{D}U}{\bar{D}t}, \tag{3.3}$$

where A is the acceleration outside the IBL. Notice that g has no dimension. In this study, we focus on a temporally evolving TBL, therefore g becomes $(\partial U/\partial t)/A$. By differentiating (3.1) with respect to time, we derive the governing equation for g:

$$\frac{\partial g}{\partial t} = \nu\frac{\partial^2 g}{\partial y^2} + \frac{\partial}{\partial y}\left(-\frac{1}{A}\frac{\partial \langle u'v' \rangle}{\partial t}\right). \tag{3.4}$$

The PG emerges as a critical flow parameter. Define

$$\zeta = -A\nu/(\tau_{w,0}/\rho)^{3/2}. \tag{3.5}$$

This parameter is analogous to the Clauser PG parameter (Clauser 1956), but instead of the displacement height, we employ the viscous length scale for non-dimensionalisation.

We see that (3.2) and (3.4) have similar forms, suggesting an analogy between the velocity U in a ZPG TBL and the fluid acceleration g in PG TBLs. In particular, since

$$U = f_1\left(\nu,\ \nu\frac{\partial U}{\partial y}\bigg|_w,\ y\right) \quad \text{for } y \ll \delta, \tag{3.6}$$

in a ZPG TBL, by the analogy, we should have

$$g = f_2\left(\nu,\ \nu\frac{\partial g}{\partial y}\bigg|_w,\ y\right) \quad \text{for } y \ll \delta, \tag{3.7}$$

in a PG TBL. Here, f_1 and f_2 are generic functions, and the subscript w denotes quantities evaluated at the wall. Applying dimensional analysis to (3.6) gives

$$U = f_1\left(\frac{y}{\nu}\sqrt{\nu\frac{\partial U}{\partial y}\bigg|_w}\right), \tag{3.8}$$

in a ZPG TBL, and similarly,

$$g = f_3(\eta), \quad \eta = \frac{\left(\nu\ \dfrac{\partial g}{\partial y}\bigg|_w\right) y}{\nu}. \tag{3.9}$$

Before we proceed further, we study the limit of P_x approaching 0, i.e. the ZPG TBL, a limit that is fairly well understood. A direct consequence of (3.3), (3.5) and (3.9) is

$$\frac{\bar{D}U^+}{\bar{D}t^+} = \zeta\ f_3(\eta) = \frac{-A\delta}{u_\tau^2}\ \frac{f_3(\eta)}{Re_\tau}. \tag{3.10}$$

where $Re_\tau = u_\tau\delta/\nu$ is the friction Reynolds number. When $P_x = 0$, $A = -u_\tau^2/\delta$ and $\bar{D}U^+/\bar{D}t^+ \sim 1/Re_\tau$, which is consistent with the result in Morrill-Winter *et al.* (2017).

3.2. *Scaling of the acceleration g and the velocity U*

We now examine (3.9). It is easy to verify that (3.9) is consistent with the Stokes solution (1.6):

$$g = \operatorname{erf}\left(\frac{\sqrt{\pi}}{2}\eta\right). \tag{3.11}$$

The Stokes solution is valid when the IBL is laminar. When the IBL becomes turbulent, we anticipate the scaling

$$g = \begin{cases} \eta & \text{for } \eta \ll 0.1, \\ \dfrac{1}{\kappa_g}\ln(\eta) + B_g & \text{for } 0.1 \ll \eta \le \mathrm{e}^{\kappa_g(1-B_g)}, \\ 1 & \text{for } \eta \ge \mathrm{e}^{\kappa_g(1-B_g)}, \end{cases} \tag{3.12}$$

mirroring the mean velocity U in a ZPG TBL. The first line in this equation is the scaling in the sublayer, which can be confirmed directly by evaluating (3.4) at the wall as follows. Because $g = 0$ at the wall, $\partial g/\partial t = 0$. Also, because $\langle u'v'\rangle = O(y^3)$, $\partial^2\langle u'v'\rangle/\partial y\,\partial t = 0$

at the wall. Consequently, (3.4) simplifies to

$$\nu \left. \frac{\partial^2 g}{\partial y^2} \right|_w = 0 \tag{3.13}$$

at the wall, leading directly to the sublayer scaling

$$g = g|_w + \left. \frac{\partial g}{\partial y} \right|_w y = \eta. \tag{3.14}$$

The second line in (3.12) is the scaling of g in the inertial layer. The two constants κ_g and B_g are analogous to the two constants κ and B in the law of the wall, albeit without implying their universality. The selection of $\eta = 0.1$ as a threshold between linear and logarithmic scaling is based on the rationale that the viscous sublayer should be unaffected by freestream conditions, necessitating $g \ll 1$ in the sublayer. With the choice $g \ll 0.1$, we have $\eta = g \ll 0.1$ in the sublayer. The exact location of transition between the linear and logarithmic scalings depends on the balance between the two terms in (3.4). When the bulk flow acceleration is dominant, the transition from the linear scaling to the viscous scaling occurs at a large η; conversely, when the turbulent term is dominant, the transition occurs at a small η – which we will verify against empirical data in § 4.2. Finally, the last line in (3.12) represents the transition from the IBL to the outside boundary layer, where the acceleration is constant. The transition location is determined by assuming that g is monotonically increasing.

The scalings of the fluid acceleration in (3.12) have implications for the scaling of the velocity. Integrating g, we should have

$$U(y, t) = U(y, t_2) + \int_{t_2}^{t} A\, g(\eta(y, t))\, \mathrm{d}t, \tag{3.15}$$

where t_2 marks the time when the IBL becomes turbulent.

4. Validation

4.1. *Validation data*

We focus on temporally evolving TBLs, employing direct numerical simulations (DNS) to examine a fully developed turbulent channel flow subjected to a suddenly imposed APG. The flow is transient and is controlled by the Reynolds number, i.e. $Re_{\tau,0} = \delta u_{\tau,0}/\nu$, and the magnitude of the APG (on top of the PG that drives the initial flow), i.e. $\Pi = P_x \delta/\tau_{w,0} + 1$. Here, δ is the channel half-height, and the subscript 0 denotes the state before the PG is applied. Table 1 tabulates the details of our DNS, including $Re_{\tau,0}$, Π, ζ, the simulation time, and the time it takes for incipient separation. The bulk flow acceleration is $A = -(P_x + \tau_{w,0})/(\rho\delta)$, and $\zeta = \Pi/Re_{\tau,0}$. Notice that $\zeta \sim Re_\tau^{-1}$ for a given PG, implying that the effects of PGs decrease with the Reynolds number (Tanarro *et al.* 2020; Deshpande *et al.* 2023). We explore two distinct Reynolds numbers, $Re_{\tau,0} = 544$ and 1000, across a range of PG forces, with Π values extending from 5 to 20. The flow maintains homogeneity in both the streamwise and spanwise directions, allowing for averages to be taken across these axes. Additionally, ensemble averages are computed from eight independent realisations to ensure statistical convergence. The numerics of our DNS code are identical to those in Lee & Moser (2015). Further details of the code can be found in Chen *et al.* (2023*b*) and Graham *et al.* (2016), and are not repeated here for brevity. The domain sizes are listed in table 1, which are larger than the minimal channel in Lozano-Durán & Jiménez (2014). Figure 2 illustrates the grid resolutions as the flow

Case	$Re_{\tau,0}$	Π	ζ	$L_x \times L_y \times L_z$	$N_x \times N_y \times N_z$	t_e^+	t_{sep}^+
R544A5	544	6	0.011	$4\pi \times 2 \times 2\pi$	$576 \times 243 \times 540$	1600	1495
R544A10	544	11	0.020	$4\pi \times 2 \times 2\pi$	$576 \times 243 \times 540$	1000	696
R544A20	544	21	0.039	$4\pi \times 2 \times 2\pi$	$576 \times 243 \times 540$	1000	304.1
R1000A10	1000	11	0.011	$8\pi \times 2 \times 3\pi$	$2048 \times 512 \times 1536$	1400	1392
R544A10-20	544	–	–	$4\pi \times 2 \times 2\pi$	$576 \times 243 \times 540$	1000	445.5

Table 1. Details of the DNS. The nomenclature is R[$Re_{\tau,0}$]A[$P_x/\tau_{w,0}$]. We list the initial Reynolds number $Re_{\tau,0} = \delta u_{\tau,0}/\nu$, the PG $\Pi = P_x\delta/\tau_{w,0} + 1$, the non-dimensional PG $\zeta = -A\nu/u_{\tau,0}^3$, the size of the computational domain L_x, L_y and L_z, the grid size N_x, N_y and N_z, and the simulation time t_e and the time until incipient separation t_{sep}. The superscript + indicates normalisation by $\nu/u_{\tau,0}^2$. For R544A10-20, Π and ζ vary, and their variations are illustrated in figure 3.

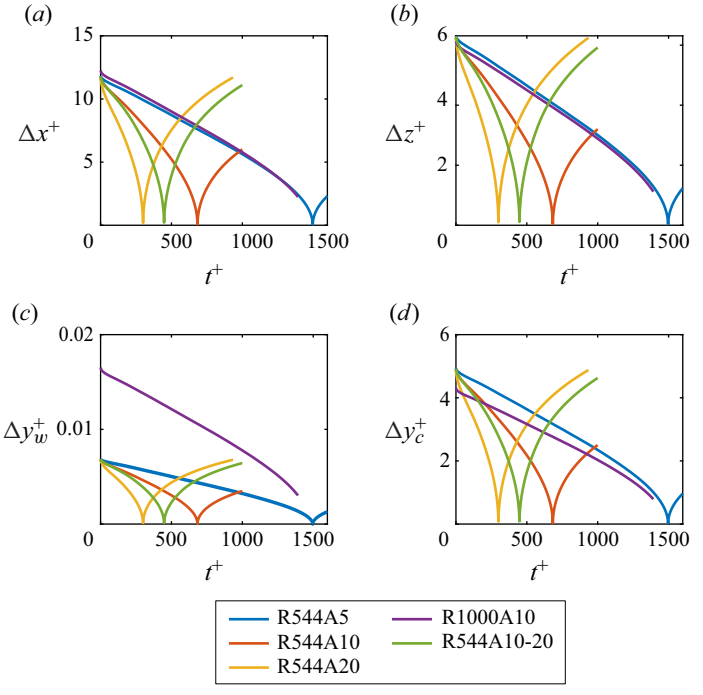

Figure 2. Grid resolution normalised with the instantaneous friction scales, i.e. $\delta_\nu(t) = \nu/\sqrt{|\tau_w|/\rho}$. Here, Δx and Δz are the grid spacings in the streamwise and spanwise directions, respectively; Δy_w is the grid spacing in the wall-normal direction at the wall, and Δy_c is the one at the centreline.

evolves, normalised using the instantaneous friction scales. The flow initially decelerates, then accelerates in the opposite direction. Throughout the entire evolution process, the grid resolutions adhere to established heuristics: $\Delta x^+ \lesssim 10$, $\Delta z^+ \lesssim 6$, $\Delta y_w^+ < 1$ and $\Delta y_c^+ \lesssim 6$ (Kim *et al.* 1987; Chen *et al.* 2023*b*).

The DNS are not the focus of the study, and here we show some relevant results. Figure 4 shows the evolution of the wall-shear stress τ_w. The times for incipient separation are listed in table 2. The flow separates earlier when a larger non-dimensional PG is applied. Notice that the R544A5 and R1000A10 results collapse in figure 4, showing the power of ζ as a controlling parameter.

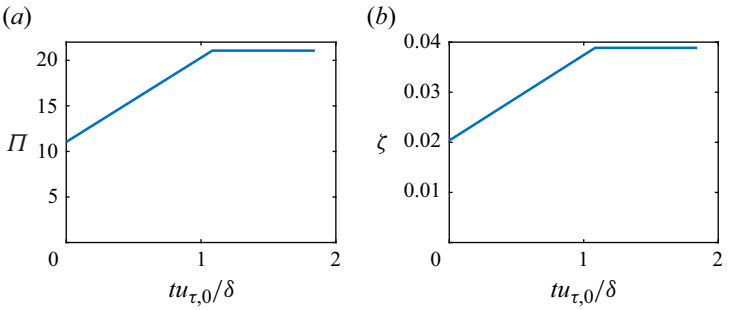

Figure 3. (*a*) The PG force $\Pi = P_x\delta/\tau_{w,0} + 1$ and (*b*) the non-dimensional PG parameter $\zeta = -A\nu/u_{\tau,0}^3$, as functions of $tu_{\tau,0}/\delta$ in R544A10-20.

Case	κ_g	B_g	t_1^+	t_2^+
R544A5	10	0.66	5×10	4×10^2
R544A10	11	0.72	5×10	3×10^2
R544A20	11	0.76	5×10	3×10^2
R1000A10	11	0.67	3×10	4×10^2
R544A10-20	11	0.75	5×10	3×10^2

Table 2. The measured κ_g and B_g. The IBL is laminar for $0 < t < t_1$, and turbulent for $t_2 < t$.

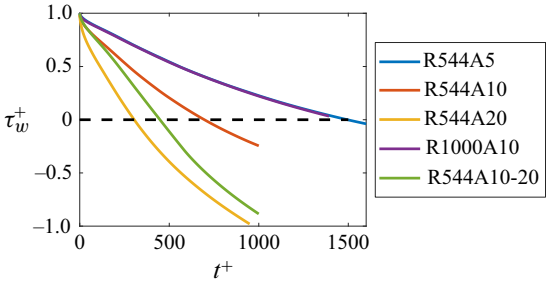

Figure 4. Evolution of the wall-shear stress in our DNS.

4.2. *Validation results*

The study has so far corroborated the analogy within the viscous sublayer through comparisons with the Stokes solution and an evaluation of the Navier–Stokes equations at the wall. Nonetheless, the validity (and the usefulness) of any analogy hinges on its validation against empirical data. To this end, we juxtapose (3.11) and (3.12) against experimental and DNS data. Here, (3.11) is equivalent to the Stokes solution and applies to laminar IBLs, i.e. $t < t_1$; (3.12) and (3.15), on the other hand, apply to turbulent IBLs, i.e. $t > t_2$. Table 2 lists the values of t_1 and t_2 for all DNS cases.

Figure 5 illustrates the flow acceleration g as a function of the non-dimensional distance from the wall η for $t < t_1$. The data closely follow (3.11). This is not unexpected as the validity of the Stokes solution for laminar IBLs is known. Next, we assess (3.12). We first present profiles of non-dimensional fluid acceleration g as a function of conventional wall-normal coordinates y^+ and y/δ in figure 6. Note that g does not collapse when plotted

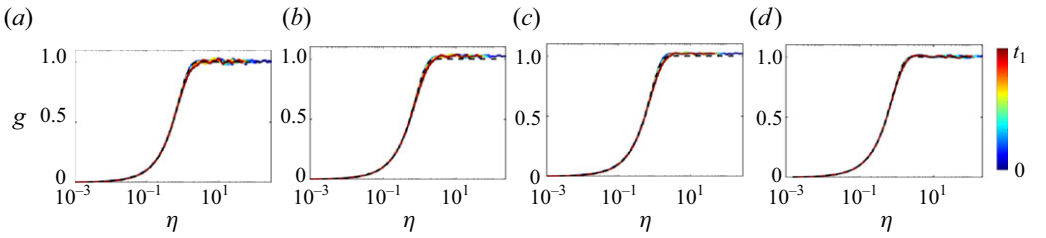

Figure 5. The non-dimensional fluid acceleration g as a function of η for $t < t_1$. The profiles are evenly sampled between $t = 0$ and $t = t_1$: (*a*) R544A5, (*b*) R544A10, (*c*) R544A20, (*d*) R1000A10. The black dashed line corresponds to (3.11).

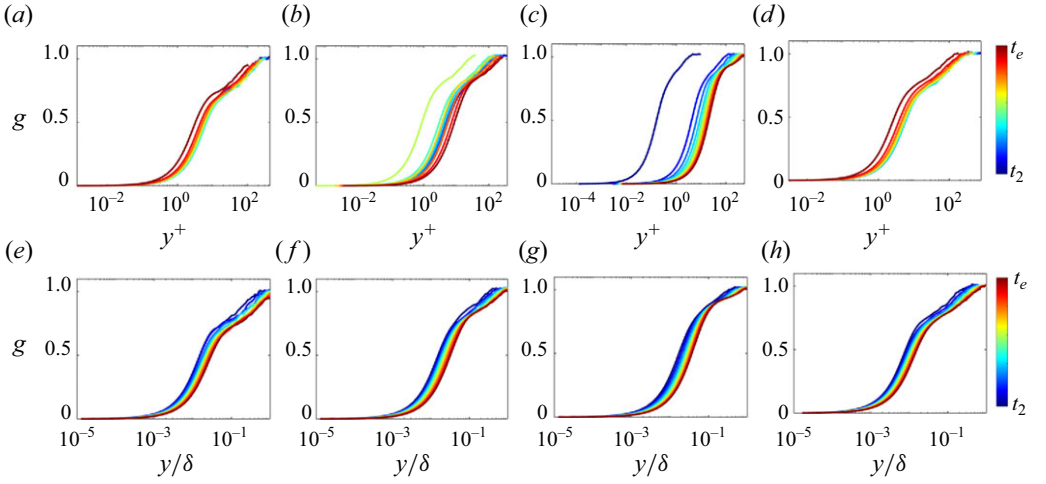

Figure 6. The fluid acceleration g as a function of (*a,b,c,d*) y^+ and (*e,f,g,h*) y/δ, for (*a,e*) R544A5, (*b,f*) R544A10, (*c,g*) R544A20, (*d,h*) R1000A10. The profiles are evenly sampled between $t = t_2$ and $t = t_e$.

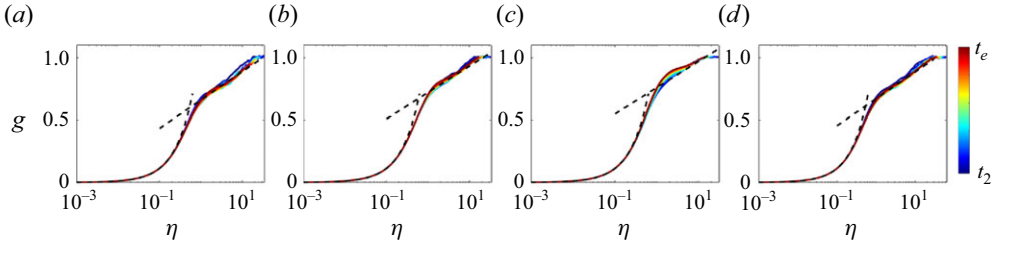

Figure 7. The fluid acceleration g as a function of η: (*a*) R544A5, (*b*) R445A10, (*c*) R544A20, (*d*) R1000A10. The black dashed lines correspond to the linear and the logarithmic scalings in (3.12). The profiles are evenly sampled between $t = t_2$ and $t = t_e$.

against either y^+ or y/δ. Figure 7 shows g as a function of η, and we see a good collapse of the profiles. In particular, g adheres to a linear scaling in the wall layer and a logarithmic one above, in accordance with (3.12). Furthermore, we see that the transition between the linear and logarithmic scalings moves away from the wall as the non-dimensional PG parameter ζ increases, corroborating the discussion in § 3.

The logarithmic scaling in (3.12) contains two parameters, κ_g and B_g, and it is instructive to determine their values. Table 2 lists the measured values of κ_g and B_g.

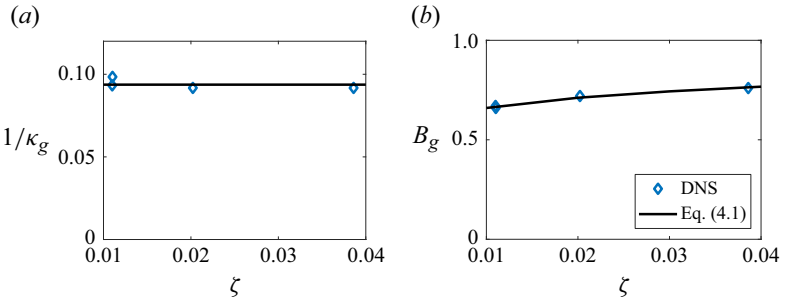

Figure 8. Plots of (*a*) $1/\kappa_g$ as a function of ζ, and(*b*) B_g as a function of ζ. In (*a*), the black solid lines represent the mean values of the four cases.

Figure 8 illustrates κ_g and B_g as functions of the non-dimensional PG parameter ζ. The data indicate that κ_g is insensitive to the flow condition, and its value is given by $1/\kappa_g \approx 0.094 \pm 0.004$. On the other hand, B_g increases slightly as a function of the non-dimensional PG parameter ζ. Its value is 0.66 when $\zeta = 0.011$, and 0.8 when $\zeta = 0.038$. The present data suggest

$$B_g = 1.1\zeta^{0.11}, \tag{4.1}$$

indicating a weak dependence on ζ.

We proceed to examine the effectiveness of the velocity scaling (3.15). Figure 9 compares (3.15) to the DNS data at a few time instants between $t = t_2$ and $t = t_e$. For comparison purposes, we have also plotted the canonical logarithmic law in (1.1), which proves to be a good approximation of the mean flow for the early times and under conditions of mild APGs. Errors emerge as the flow evolves in R544A10, and particularly in R544A20. In the latter, intense flow deceleration results in flow separation. Consequently, the flow in the wall layer reverses, and is responsible for the significant errors in the canonical logarithmic law. The scaling in (3.15), on the other hand, is accurate across the board, including that leading to flow separation.

For completeness, we show g as a function of η for $t_1 < t < t_2$ in figure 10. The Stokes solution and the logarithmic scaling in (3.12) are plotted for reference purposes. Here, we see that the flow acceleration g converges from the Stokes solution to the logarithmic scaling.

4.3. *Varying PGs*

The analogy is formally developed for constant PGs, and its validity is likewise so restricted. In this subsection, we study the behaviours of fluid acceleration in a TBL with slowly varying PGs, i.e. case R544A10-20, and test if the analogy extrapolates to cases with a varying PG. Like the other cases in table 1, the flow in R544A10-20 is a fully developed channel flow at $t = 0$. The following APG is then imposed:

$$\Pi = \begin{cases} 11 + 10tu_{\tau,0}/\delta & \text{for } t < \delta/u_{\tau,0}, \\ 21 & \text{for } t > \delta/u_{\tau,0}. \end{cases} \tag{4.2}$$

Notice that the PG doubles over one large-eddy turnover time. We proceed to compare the scalings in (3.11) and (3.12) to data. Figure 11 shows the flow acceleration g as a function of η for $t < t_1$, $t_1 < t < t_2$ and $t_2 < t$, i.e. when the IBL is laminar, transitional and turbulent. The data follow the laminar Stokes solution when the IBL is laminar, and the DNS data converge to the scaling in (3.12) as the IBL transitions to turbulence.

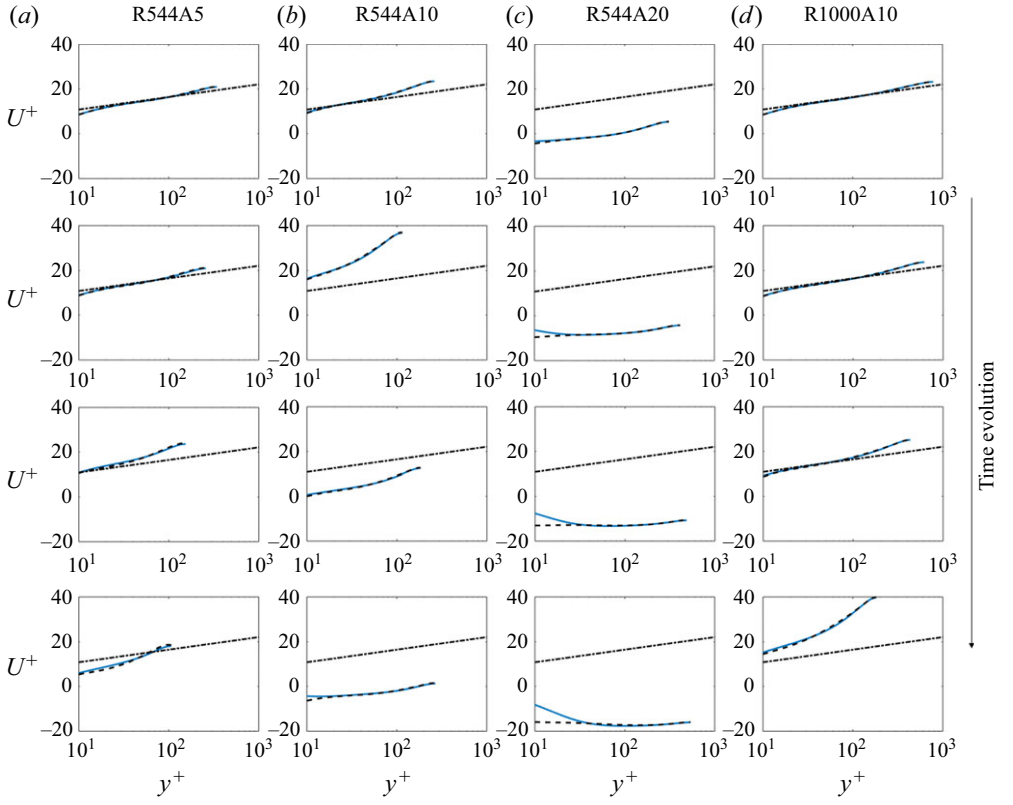

Figure 9. Velocity U^+ as a function of y^+ at a few time instants between $t = t_2$ and $t = t_e$: (*a*) R544A5, (*b*) R544A10, (*c*) R544A20, (*d*) R1000A10. The dashed lines and the dot-dashed lines correspond to the reference scalings in (3.15) and the canonical law of the wall.

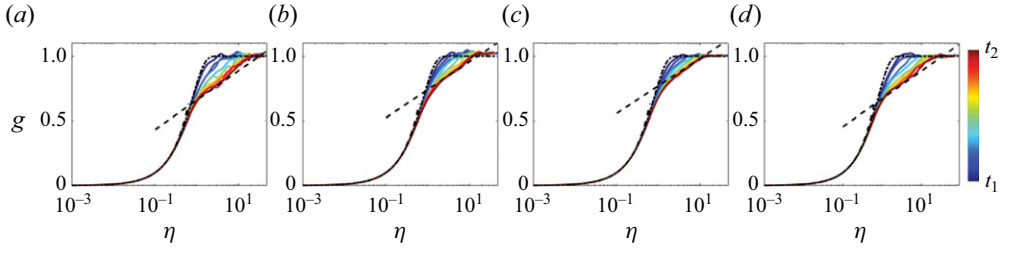

Figure 10. The fluid acceleration g as a function of η for $t_1 < t < t_2$: (*a*) R544A5, $\zeta = 0.011$; (*b*) R544A10, $\zeta = 0.020$; (*c*) R544A20, $\zeta = 0.039$; (*d*) R1000A10, $\zeta = 0.011$. The black dashed lines correspond to the two reference scalings in (3.11) and (3.12).

In particular, we see from figure 11(*c*) a logarithmic region in the fluid acceleration. The values of the two constants are $\kappa_g = 10.90$ and $B_g = 0.75$, which are not far from the values in cases R544A10 and R544A20. We further compare the velocity scaling in (3.15) to data; figure 12 shows the results. The canonical law of the wall is included for comparison purposes. The result is similar to that in § 4.2: the canonical log law is accurate initially, but becomes increasingly inaccurate as the flow evolves, whereas the scaling in (3.15) remains accurate. Hence we conclude that the log-layer analogy developed here is applicable to TBLs with slowly varying PGs.

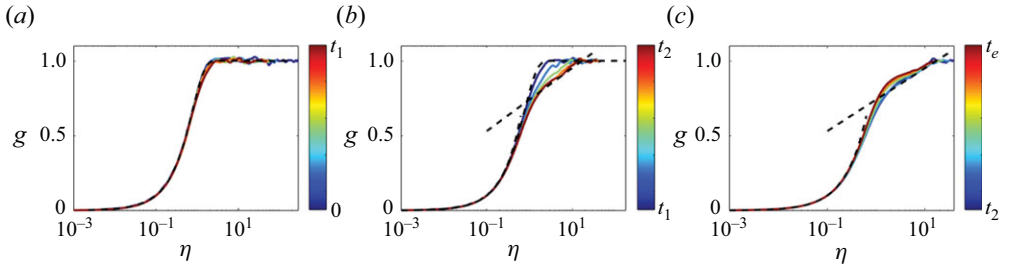

Figure 11. The non-dimensional flow acceleration g as a function of η for (*a*) $t < t_1$, (*b*) $t_1 < t < t_2$, (*c*) $t_2 < t < t_e$. In (*a*), the black dashed line corresponds to the reference scaling (3.11); (*b*) (3.11) and (3.12); (*c*) (3.12).

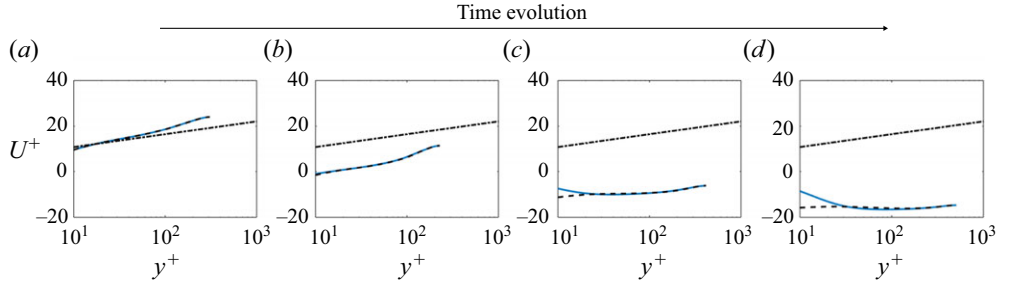

Figure 12. The non-dimensional velocity U^+ as a function of y^+ at a few time instants between $t = t_2$ and $t = t_e$, for R544A10-20. The dashed lines and dot-dashed lines correspond to the reference scalings in (3.15) and the canonical law of the wall.

5. Conclusions

In the current study, we establish an analogy between the inner layer of equilibrium spatially evolving boundary layers and that of temporally evolving boundary layers with pressure gradients (PGs) by drawing parallels between their governing transport equations. Specifically, we compare the transport equation for velocity in the spatially evolving case with the transport equation for fluid acceleration in the temporally evolving scenario. As previous work has focused on velocity analysis, this study provides a new perspective. Exploiting the log-layer analogy, we drew the following conclusions. First, the fluid acceleration is a function of $\eta = (\nu\, \partial g/\partial y)_w\, y/\nu$ in (3.9). Second, analogous to the logarithmic law for velocity, fluid acceleration should exhibit similar scaling behaviours in turbulent IBLs (3.12). Since the integration of acceleration leads to the velocity scaling (3.15), the scaling of the fluid acceleration has implications for the velocity scaling. Third, the non-dimensionalised PG force $\zeta = -A\nu/(\tau_{w,0}/\rho)^{3/2}$ emerges as an important parameter, suggesting that flows with similar ζ values exhibit similar behaviours. Empirical validation of this analogy was pursued through comparisons with the Stokes solution for laminar flows immediately after the application of a PG, and through direct numerical simulations of fully developed channel flows under suddenly imposed adverse PGs. These comparisons yielded highly favourable outcomes, supporting the analogy's applicability. Nonetheless, by focusing on the channel configuration and maintaining the channel half-height, the present work neglects the impacts of varying outer length scales. Therefore, its applicability to boundary layer flows is yet to be tested, a topic left for future investigation.

Funding. We acknowledge the support from NSFC (grant nos 11988102, 12102168, 12225204), Shenzhen Science & Technology Program (grant no. KQTD20180411143441009), Department of Science and Technology

of Guangdong Province (grant nos 2023B1212060001, 2020B1212030001). X.I.A.Y. acknowledges Office of Naval Research, grant no. N000142012315.

Declaration of interests. The authors report no conflict of interest.

Data availability statement. The data that support the findings of this study are available from the corresponding author upon reasonable request.

References

ALVING, A.E. & FERNHOLZ, H.H. 1995 Mean-velocity scaling in and around a mild, turbulent separation bubble. *Phys. Fluids* **7** (8), 1956–1969.

BAILEY, S.C.C. *et al.* 2013 Obtaining accurate mean velocity measurements in high Reynolds number turbulent boundary layers using Pitot tubes. *J. Fluid Mech.* **715**, 642–670.

BASKARAN, V., SMITS, A.J. & JOUBERT, P.N. 1987 A turbulent flow over a curved hill. Part 1. Growth of an internal boundary layer. *J. Fluid Mech.* **182**, 47–83.

BOBKE, A., VINUESA, R., ÖRLÜ, R. & SCHLATTER, P. 2017 History effects and near equilibrium in adverse-pressure-gradient turbulent boundary layers. *J. Fluid Mech.* **820**, 667–692.

BOSE, S.T. & PARK, G.I. 2018 Wall-modeled large-eddy simulation for complex turbulent flows. *Ann. Rev. Fluid Mech.* **50** (1), 535–561.

BRADSHAW, P. 1974 Possible origin of Prandtl's mixing-length theory. *Nature* **249** (5453), 135–136.

BRUCKER, K.A. & SARKAR, S. 2010 A comparative study of self-propelled and towed wakes in a stratified fluid. *J. Fluid Mech.* **652**, 373–404.

DE BRUYN KOPS, S.M. & RILEY, J.J. 2019 The effects of stable stratification on the decay of initially isotropic homogeneous turbulence. *J. Fluid Mech.* **860**, 787–821.

CHEN, P.E.S., WU, W., GRIFFIN, K.P., SHI, Y. & YANG, X.I.A. 2023*a* A universal velocity transformation for boundary layers with pressure gradients. *J. Fluid Mech.* **970**, A3.

CHEN, P.E.S., ZHU, X., SHI, Y. & YANG, X.I.A. 2023*b* Quantifying uncertainties in direct-numerical-simulation statistics due to wall-normal numerics and grids. *Phys. Rev. Fluids* **8** (7), 074602.

CLAUSER, F.H. 1954 Turbulent boundary layers in adverse pressure gradients. *J. Atmos. Sci.* **21** (2), 91–108.

CLAUSER, F.H. 1956 The turbulent boundary layer. *Adv. Appl. Mech.* **4**, 1–51.

COLEMAN, G.N., KIM, J. & SPALART, P.R. 2000 A numerical study of strained three-dimensional wall-bounded turbulence. *J. Fluid Mech.* **416**, 75–116.

COLEMAN, G.N., KIM, J. & SPALART, P.R. 2003 Direct numerical simulation of a decelerated wall-bounded turbulent shear flow. *J. Fluid Mech.* **495**, 1–18.

COLEMAN, G.N., RUMSEY, C.L. & SPALART, P.R. 2018 Numerical study of turbulent separation bubbles with varying pressure gradient and Reynolds number. *J. Fluid Mech.* **847**, 28–70.

DESHPANDE, R., VAN DEN BOGAARD, A., VINUESA, R., LINDIĆ, L. & MARUSIC, I. 2023 Reynolds-number effects on the outer region of adverse-pressure-gradient turbulent boundary layers. *Phys. Rev. Fluids* **8** (12), 124604.

DRÓŻDŻ, A., ELSNER, W. & DROBNIAK, S. 2015 Scaling of streamwise Reynolds stress for turbulent boundary layers with pressure gradient. *Eur. J. Mech. B/Fluids* **49**, 137–145.

EL TELBANY, M.M.M. & REYNOLDS, A.J. 1980 Velocity distributions in plane turbulent channel flows. *J. Fluid Mech.* **100** (1), 1–29.

GALBRAITH, R.A.M.D., SJOLANDER, S. & HEAD, M.R. 1977 Mixing length in the wall region of turbulent boundary layers. *Aeronaut. Q.* **28** (2), 97–110.

GARRATT, J.R. 1990 The internal boundary layer – a review. *Boundary-Layer Meteorol.* **50** (1–4), 171–203.

GEORGE, W.K. & CASTILLO, L. 1997 Zero-pressure-gradient turbulent boundary layer. *Appl. Mech. Rev.* **50** (12), 689–729.

GRAHAM, J. *et al.* 2016 A web services accessible database of turbulent channel flow and its use for testing a new integral wall model for LES. *J. Turbul.* **17** (2), 181–215.

GUERRERO, B., LAMBERT, M.F. & CHIN, R.C. 2023 Transient behaviour of decelerating turbulent pipe flows. *J. Fluid Mech.* **962**, A44.

HE, K., SEDDIGHI, M. & HE, S. 2016 DNS study of a pipe flow following a step increase in flow rate. *Intl J. Heat Fluid Flow* **57**, 130–141.

HE, S. & SEDDIGHI, M. 2013 Turbulence in transient channel flow. *J. Fluid Mech.* **715**, 60–102.

HE, S. & SEDDIGHI, M. 2015 Transition of transient channel flow after a change in Reynolds number. *J. Fluid Mech.* **764**, 395–427.

JOHNSTONE, R., COLEMAN, G.N. & SPALART, P.R. 2010 The resilience of the logarithmic law to pressure gradients: evidence from direct numerical simulation. *J. Fluid Mech.* **643**, 163–175.

KADER, B.A. & YAGLOM, A.M. 1978 Similarity treatment of moving-equilibrium turbulent boundary layers in adverse pressure gradients. *J. Fluid Mech.* **89** (2), 305–342.
KAYS, W.M., CRAWFORD, M.E. & WEIGAND, B. 1980 *Convective Heat and Mass Transfer*. McGraw-Hill.
KIM, J., MOIN, P. & MOSER, R. 1987 Turbulence statistics in fully developed channel flow at low Reynolds number. *J. Fluid Mech.* **177**, 133–166.
KNOPP, T. 2022 An empirical wall law for the mean velocity in an adverse pressure gradient for RANS turbulence modelling. *Flow Turbul. Combust.* **109** (3), 571–601.
KNOPP, T., REUTHER, N., NOVARA, M., SCHANZ, D., SCHÜLEIN, E., SCHRÖDER, A. & KÄHLER, C.J. 2021 Experimental analysis of the log law at adverse pressure gradient. *J. Fluid Mech.* **918**, A17.
KOZUL, M., CHUNG, D. & MONTY, J.P. 2016 Direct numerical simulation of the incompressible temporally developing turbulent boundary layer. *J. Fluid Mech.* **796**, 437–472.
LEE, J.H. 2017 Large-scale motions in turbulent boundary layers subjected to adverse pressure gradients. *J. Fluid Mech.* **810**, 323–361.
LEE, J.-H. & SUNG, H.J. 2009 Structures in turbulent boundary layers subjected to adverse pressure gradients. *J. Fluid Mech.* **639**, 101–131.
LEE, M. & MOSER, R.D. 2015 Direct numerical simulation of turbulent channel flow up to $Re_\tau \approx 5200$. *J. Fluid Mech.* **774**, 395–415.
LI, J.J.L., YANG, X.I.A. & KUNZ, R.F. 2024 Direct numerical simulation of temporally evolving stratified wakes with ensemble average. *J. Fluid Mech.* **980**, A3.
LI, M., DE SILVA, C.M., CHUNG, D., PULLIN, D.I., MARUSIC, I. & HUTCHINS, N. 2022 Modelling the downstream development of a turbulent boundary layer following a step change of roughness. *J. Fluid Mech.* **949**, A7.
LOZANO-DURÁN, A., GIOMETTO, M.G., PARK, G.I. & MOIN, P. 2020 Non-equilibrium three-dimensional boundary layers at moderate Reynolds numbers. *J. Fluid Mech.* **883**, A20.
LOZANO-DURÁN, A. & JIMÉNEZ, J. 2014 Effect of the computational domain on direct simulations of turbulent channels up to $Re_\tau = 4200$. *Phys. Fluids* **26** (1), 011702.
LUCHINI, P. 2017 Universality of the turbulent velocity profile. *Phys. Rev. Lett.* **118** (22), 224501.
LV, Y., HUANG, X.L.D., YANG, X & YANG, X.I.A. 2021 Wall-model integrated computational framework for large-eddy simulations of wall-bounded flows. *Phys. Fluids* **33** (12), 125120.
MARUSIC, I., MONTY, J.P., HULTMARK, M. & SMITS, A.J. 2013 On the logarithmic region in wall turbulence. *J. Fluid Mech.* **716**, R3.
MATERNY, M., DRÓŻDŻ, A., DROBNIAK, S. & ELSNER, W. 2008 Experimental analysis of turbulent boundary layer under the influence of adverse pressure gradient. *Arch. Mech.* **60** (6), 449–466.
MATHUR, A., GORJI, S., HE, S., SEDDIGHI, M., VARDY, A.E., O'DONOGHUE, T. & POKRAJAC, D. 2018 Temporal acceleration of a turbulent channel flow. *J. Fluid Mech.* **835**, 471–490.
MELLOR, G.L. & GIBSON, D.M. 1966 Equilibrium turbulent boundary layers. *J. Fluid Mech.* **24** (2), 225–253.
MONKEWITZ, P.A. & NAGIB, H.M. 2023 The hunt for the Kármán 'constant' revisited. *J. Fluid Mech.* **967**, A15.
MONTY, J.P., HARUN, Z. & MARUSIC, I. 2011 A parametric study of adverse pressure gradient turbulent boundary layers. *Intl J. Heat Fluid Flow* **32** (3), 575–585.
MORRILL-WINTER, C., PHILIP, J. & KLEWICKI, J. 2017 An invariant representation of mean inertia: theoretical basis for a log law in turbulent boundary layers. *J. Fluid Mech.* **813**, 594–617.
PARTHASARATHY, A. & SAXTON-FOX, T. 2023 A family of adverse pressure gradient turbulent boundary layers with upstream favourable pressure gradients. *J. Fluid Mech.* **966**, A11.
PERRY, A.E., BELL, J.B. & JOUBERT, P.N. 1966 Velocity and temperature profiles in adverse pressure gradient turbulent boundary layers. *J. Fluid Mech.* **25** (2), 299–320.
POPE, S.B. 2000 *Turbulent Flows*. Cambridge University Press.
POZUELO, R., LI, Q., SCHLATTER, P. & VINUESA, R. 2022 An adverse-pressure-gradient turbulent boundary layer with nearly constant $\beta \approx 1.4$ up to $Re_\theta \approx 8700$. *J. Fluid Mech.* **939**, A34.
PRANDTL, L. 1925 A report on testing for built-up turbulence. *Z. Angew. Math. Mech.* **5** (2), 136–139.
RAUPACH, M.R., FINNIGAN, J.J. & BRUNET, Y. 1996 Coherent eddies and turbulence in vegetation canopies: the mixing-layer analogy. *Boundary-Layer Meteorol.* **78** (3–4), 351–382.
ROMERO, S., ZIMMERMAN, S., PHILIP, J., WHITE, C. & KLEWICKI, J. 2022*a* Properties of the inertial sublayer in adverse pressure-gradient turbulent boundary layers. *J. Fluid Mech.* **937**, A30.
ROMERO, S.K., ZIMMERMAN, S.J., PHILIP, J. & KLEWICKI, J.C. 2022*b* Stress equation based scaling framework for adverse pressure gradient turbulent boundary layers. *Intl J Heat Fluid Flow* **93**, 108885.
SANMIGUEL VILA, C., ÖRLÜ, R., VINUESA, R., SCHLATTER, P., IANIRO, A. & DISCETTI, S. 2017 Adverse-pressure-gradient effects on turbulent boundary layers: statistics and flow-field organization. *Flow Turbul. Combust.* **99** (3–4), 589–612.

SCHLATTER, P., ÖRLÜ, R., LI, Q., BRETHOUWER, G., FRANSSON, J.H.M., JOHANSSON, A.V., ALFREDSSON, P.H. & HENNINGSON, D.S. 2009 Turbulent boundary layers up to $Re_\theta = 2500$ studied through simulation and experiment. *Phys. Fluids* **21** (5), 51702.

SCHLICHTING, H. & GERSTEN, K. 2016 *Boundary-Layer Theory*. Springer.

SIMPSON, R.L. 1989 Turbulent boundary-layer separation. *Annu. Rev. Fluid Mech.* **21** (1), 205–232.

SKOTE, M., HENNINGSON, D.S. & HENKES, R.A.W.M. 1998 Direct numerical simulation of self-similar turbulent boundary layers in adverse pressure gradients. *Flow Turbul. Combust.* **60** (1), 47–85.

SMITS, A.J., MCKEON, B.J. & MARUSIC, I. 2011 High-Reynolds number wall turbulence. *Ann. Rev. Fluid Mech.* **43** (1), 353–375.

SMITS, A.J. & WOOD, D.H. 1985 The response of turbulent boundary layers to sudden perturbations. *Ann. Rev. Fluid Mech.* **17** (1), 321–358.

SO, R.M.C. & SPEZIALE, C.G. 1999 A review of turbulent heat transfer modeling. *Annu. Rev. Heat Transfer* **10** (10), 177–220.

SPALART, P.R. & WATMUFF, J.H. 1993 Experimental and numerical study of a turbulent boundary layer with pressure gradients. *J. Fluid Mech.* **249**, 337–371.

DE STADLER, M.B., SARKAR, S. & BRUCKER, K.A. 2010 Effect of the Prandtl number on a stratified turbulent wake. *Phys. Fluids* **22** (9), 095102.

STRATFORD, B.S. 1959 The prediction of separation of the turbulent boundary layer. *J. Fluid Mech.* **5** (1), 1–16.

SUBRAHMANYAM, M.A., CANTWELL, B.J. & ALONSO, J.J. 2022 A universal velocity profile for turbulent wall flows including adverse pressure gradient boundary layers. *J. Fluid Mech.* **933**, A16.

TANARRO, Á., VINUESA, R. & SCHLATTER, P. 2020 Effect of adverse pressure gradients on turbulent wing boundary layers. *J. Fluid Mech.* **883**, A8.

TAYLOR, P.S. & SEDDIGHI, M. 2024 Turbulent–turbulent transient concept in pulsating flows. *J. Fluid Mech.* **982**, A20.

TOWNSEND, A.A.R. 1976 *The Structure of Turbulent Shear Flow*. Cambridge University Press.

VINUESA, R., ÖRLÜ, R., SANMIGUEL VILA, C., IANIRO, A., DISCETTI, S. & SCHLATTER, P. 2017 Revisiting history effects in adverse-pressure-gradient turbulent boundary layers. *Flow Turbul. Combust.* **99** (3–4), 565–587.

VINUESA, R., ROZIER, P.H., SCHLATTER, P. & NAGIB, H.M. 2014 Experiments and computations of localized pressure gradients with different history effects. *AIAA J.* **52** (2), 368–384.

VISHWANATHAN, V., FRITSCH, D.J., LOWE, K.T. & DEVENPORT, W.J. 2023 History effects and wall-similarity of non-equilibrium turbulent boundary layers in varying pressure gradient over rough and smooth surfaces. *Intl J. Heat Fluid Flow* **102**, 109145.

VOLINO, R.J. 2020 Non-equilibrium development in turbulent boundary layers with changing pressure gradients. *J. Fluid Mech.* **897**, A2.

WEI, T., LI, Z., KNOPP, T. & VINUESA, R. 2023 The mean wall-normal velocity in turbulent boundary layer flows under pressure gradient. *J. Fluid Mech.* **975**, A27.

YANG, X.I.A., SADIQUE, J., MITTAL, R. & MENEVEAU, C. 2015 Integral wall model for large eddy simulations of wall-bounded turbulent flows. *Phys. Fluids* **27** (2), 025112.

ZHANG, W., ZHU, X., YANG, X.I.A. & WAN, M. 2022 Evidence for Raupach *et al.*'s mixing-layer analogy in deep homogeneous urban-canopy flows. *J. Fluid Mech.* **944**, A46.